fluids

MDPI

Article

A Study of the Dependence of the Mach Stem Height on the Trailing Edge Height

Chen-Yuan Bai [1,†] and Zi-Niu Wu [2,*,†]

[1] Ministry of Education Key Laboratory of Fluid Mechanics, School of Aeronautic Science and Engineering, Beihang University, Beijing 100191, China; baicy@buaa.edu.cn
[2] Department of Engineering Mechanics, Tsinghua University, Beijing 100084, China
* Correspondence: ziniuwu@tsinghua.edu.cn
† These authors contributed equally to this work.

Abstract: The Mach stem height is an important parameter in the Mach reflection of steady supersonic flow. Various experimental, numerical, and theoretical works have been conducted to study this parameter in the past. However, much of the established work focuses around a single set of trailing edge heights. Here, we perform a study to show the dependence of Mach stem height on the trailing edge height for a wider range of geometry. Through numerical simulation for a set of trailing edge heights, we found that the normalized Mach stem height is almost linear with respect to the normalized wedge trailing edge height. The parameter used for normalization can be either the inlet height or the length of the lower wedge surface. The observation of this linear trend is justified through a simplified analysis, which leads to an expression of the Mach stem height that linearly depends on the trailing edge height. The present study extends our knowledge about how the geometry affects the Mach stem height, and provides a basis for future work to elaborate analytical models for Mach stem height.

Keywords: gas dynamics; shock waves; shock reflection

check for updates

Citation: Bai, C.-Y.; Wu, Z.-N. A Study of the Dependence of the Mach Stem Height on the Trailing Edge Height. *Fluids* **2021**, *6*, 313. https://doi.org/10.3390/fluids6090313

Academic Editor: Olga A. Azarova

Received: 2 August 2021
Accepted: 25 August 2021
Published: 2 September 2021

Publisher's Note: MDPI stays neutral with regard to jurisdictional claims in published maps and institutional affiliations.

Copyright: © 2021 by the authors. Licensee MDPI, Basel, Switzerland. This article is an open access article distributed under the terms and conditions of the Creative Commons Attribution (CC BY) license (https://creativecommons.org/licenses/by/4.0/).

1. Introduction

Shock reflection is an important phenomenon in high-speed flow [1]. Both regular reflection and Mach reflection are possible, and the conditions to have regular reflection and Mach reflection and their transition have been well studied [1–11]. For instance, the regions of various forms of reflection were defined for both air and nitrogen by Bazhenova, Fokeev and Gvozdeva [3].

Figure 1 is a schematic configuration of a typical Mach reflection with some necessary details. The incident shock wave (i), produced by the wedge (with wedge angle θ_w) in supersonic flow (with Mach number M_0), reflects over the reflecting surface to produce a reflected shock wave (r), a Mach stem (m) and a slipline (s). These four discontinuities are connected by a point (T), known as the triple point. The flow region behind the Mach stem, bounded by the slipline and the reflecting surface, forms a flow duct that is initially convergent since the slipline deflects towards the reflecting surface near point T.

The size of the Mach stem in the case of Mach reflection has received great interest. The mechanism by which the size of a Mach reflection can be estimated is an issue raised long ago by Courant and Friedrichs [12] and Liepmann and Roshko [13]. This issue was considered to be unsolved prior to the 1990s [14–16]. Chow and Chang [17] proposed an integral approach to estimate the Mach stem height for a slightly different problem where Mach reflection lies in an over-expanded jet flow outside of a nozzle. Hornung and Robinson [18] performed an experimental study for the Mach stem height, and proposed a mechanism by which the size of the Mach stem is determined. They pointed out that the pressure decreasing information from the wedge trailing edge expansion fan is carried out to the quasi-one-dimensional flow duct, which then moves upstream through the subsonic

pocket to adjust the position of the triple point, or the Mach stem height. They pointed out a functional form of the Mach stem height and proposed that the normalized Mach stem height depends on M_0, θ_w, γ (ratio of specific heats) and g/w (trailing edge height g normalized by the wedge length w). If viscosity is accounted for, a boundary layer is attached to the wedge surface. Schmisseur and Gaitonde [19] used numerical simulation to show that this boundary layer increases the Mach stem height, due to the increased displacement effect of the wedge boundary-layer to increase the effective shock angle.

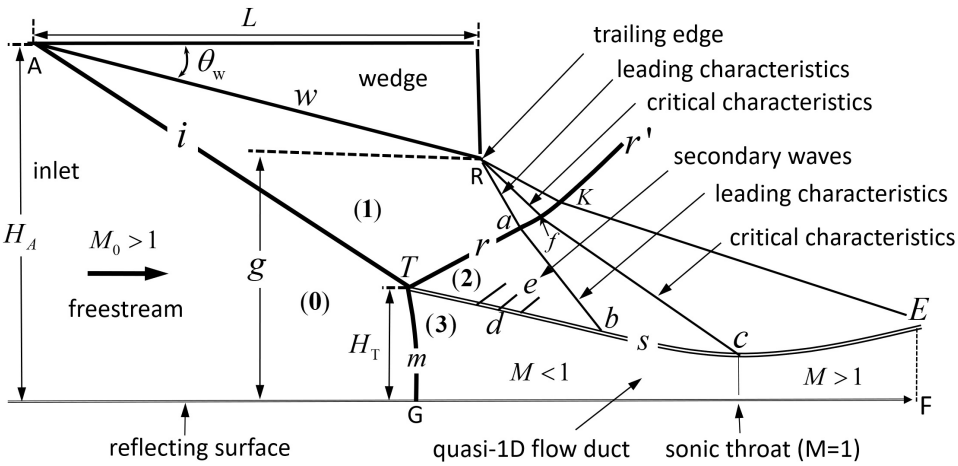

Figure 1. Mach reflection configuration. The inflow Mach number M_0, the wedge angle θ_w, the inlet height H_A and the lower wedge surface length w or the trailing edge height g are given conditions.

Since the 1990s, various attempts have been made to derive simplified models for predicting the Mach stem height [16,20,21]. A key issue in these models is how the pressure variation inside the expansion fan of the trailing edge (R) is carried out to the slipline, particularly to the sonic throat, where the height of the duct is minimal and related to the Mach stem height through the quasi-one-dimensional area Mach number relation plus the isentropic flow relation for pressure. Azevedo and Liu [20] assumed the sonic throat to be at point b, where the leading characteristics of the transmitted expansion waves intersects with the slipline. Li and Ben-Dor [16] allowed the sonic throat to be determined by the transmitted expansion waves, using the assumption that the flow just above the sonic throat is parallel to the free stream flow. This assumption was later adopted by Mouton and Hornung [21], who improved the model of Azevedo and Liu [20] and determined the Mach stem height using an unsteady approach. In the work of Azevedo and Liu [20], Li and Ben-Dor [16] and Mouton and Hornung [21], the slipline ahead of point b is treated as a straight line. Gao and Wu [22] and Bai and Wu [23] considered secondary generated expansion waves on the initial part of the slipline and demonstrated that the Mach stem height is sensitive to these pressure waves. Including the influence of these expansion waves appears to greatly increase the accuracy of the modeling. Recently, these works were extended to asymmetric shock reflection [24,25].

For symmetrical Mach reflection, past studies have shown how the Mach stem height depends on the inflow Mach number and the wedge angle. The normalized Mach stem height is a decreasing function of the inflow Mach number (Gao and Wu [22], Figure14a,b) and is an increasing function of the wedge angle or shock angle (Gao and Wu [22], Figure 14c,d, as can also be seen in Hornung and Robinson [18]). However, much of the established literature studying Mach stem height focused art approximately $g/w = 0.4$ [16,18,20–23], and the influence of a geometric setup on shock reflection was considered in the transition study [6,16]. It is thus desirable to study the Mach stem height for a wide range of geometry.

In this paper, we will use numerical simulation by computational fluid dynamics (CFD) to show that the normalized Mach stem height is almost a linear function of the normalized wedge height (Section 2). We then use some assumptions to derive a simplified

expression for the Mach stem height, to show that this linearity can be predicted even with a simplified analysis (Section 3). Finally, we make our conclusions.

In the following, M is the Mach number, p is the pressure, θ is the flow deflection angle with respect to the free-stream direction which is positive when deflected to towards the reflecting surface, β is the shock angle, and γ is the ratio of specific heats.

2. Numerical Simulation for Dependence of Mach Stem Height on the Trailing Edge Height

Numerical results for Mach stem height are obtained through solving the full set of nonlinear Euler equations in gas dynamics, using the second-order Roe scheme based on finite difference approximation and second-order upwinding for the flux [26]. The grid number we used is 400×600, which is two times denser than the grid used by Gao and Wu [22] for similar purposes.

To ensure the accuracy of CFD computation, we performed calculations using various grid densities or accuracy for $\frac{g}{H_A} = 0.6$ or $\frac{g}{w} = 0.634$ or $\frac{H_A}{w} = 1.05$, when $M_0 = 4$, $\theta_w = 25°$. The Mach contours with four different density of grids are displayed in Figure 2.

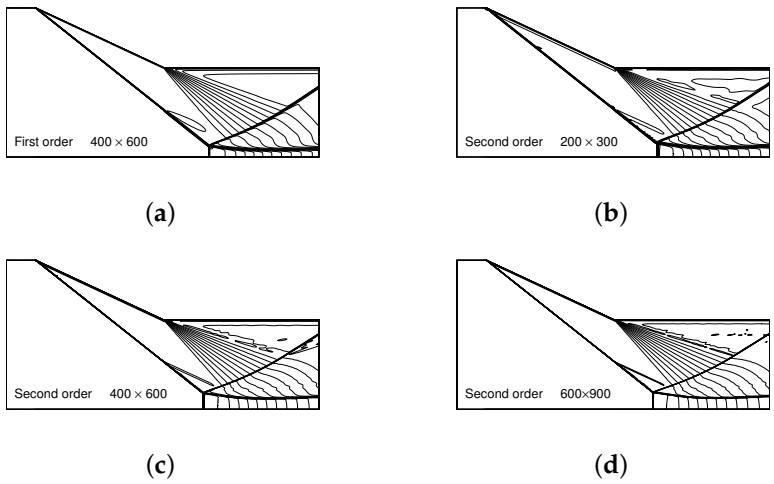

Figure 2. Mach number contours for $M_0 = 4$, $\theta_w = 25°$ and $\frac{g}{H_A} = 0.6$: (**a**) first order with a 400×600 mesh; (**b**) second order with a 200×300 mesh; (**c**) second order with a 400×600 mesh; and (**d**) second order with a 600×900 mesh.

It can be seen that the global flow structures are similar, but the Mach stem height with first-order accurate method with a grid 400×600 and second order method with a coarse grid 200×300 yield a Mach stem height much lower than that with the second order accurate method with grids 400×600 and 600×900. Moreover, the second order method with grids 400×600 and 600×900 results in Mach stem heights that are marginally close. Thus, we will use a second-order method with a grid 400×600 for simulations, since it needs less computational time than with the grid 600×900.

Now we display in Figure 3 the numerical results of normalized Mach stem height as a function of the normalized wedge trailing height for several different values of the inflow Mach number and wedge angle.

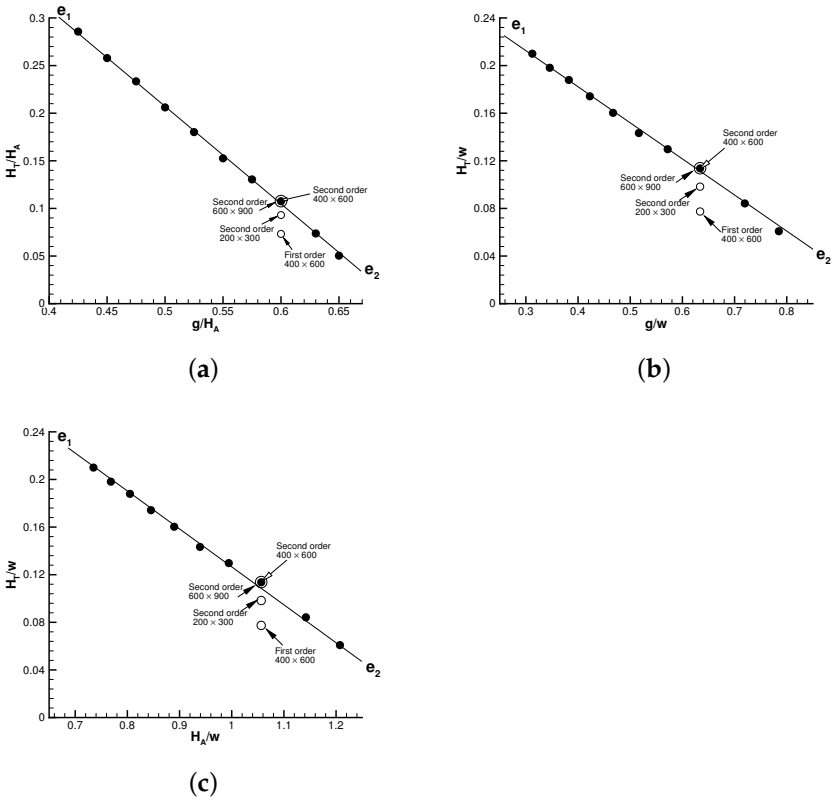

Figure 3. Numerical results for normalized Mach stem heights as a function of the normalized wedge trailing edge height for $M_0 = 4$ and $\theta_w = 25°$: (**a**) $\frac{H_T}{H_A}$ versus $\frac{g}{H_A}$; (**b**) $\frac{H_T}{w}$ versus $\frac{g}{w}$; (**c**) $\frac{H_T}{w}$ versus $\frac{H_A}{w}$. The line e_1e_2 is a straight line passing through the CFD data. Open circles are CFD data obtained using grids different to 400×600 points or a first-order accurate method.

Figure 3a displays the variation of $\frac{H_T}{H_A}$ with respect to $\frac{g}{H_A}$, for $M_0 = 4$, $\theta_w = 25°$ and a set of $\frac{g}{H_A}$ varying from 0.425 to 0.65. Figure 3b is the result for $\frac{H_T}{w}$ for various $\frac{g}{w}$, with $M_0 = 4$, $\theta_w = 25°$ and a set of $\frac{g}{w}$ varying from 0.3124 to 0.7849. Figure 3c displays the variation of $\frac{H_T}{w}$ versus $\frac{H_A}{w}$ for $M_0 = 4$, $\theta_w = 25°$ and a set of $\frac{H_A}{w}$ varying from 0.735 to 1.2075. The additional marks in Figure 3 show that numerical results with a grid of 400×600 points and with second order of accuracy are acceptable since further refining the grid does not change the Mach stem height. This supports the previous claim that the use of a second-order method with the grid 400×600 is accurate enough.

We observe that, for the conditions tested, the normalized Mach stem height $\frac{H_T}{H_A}$ is almost linear with respect to $\frac{g}{H_A}$, the normalized Mach stem height $\frac{H_T}{w}$ is almost linear with respect to $\frac{g}{w}$, and the normalized Mach stem height $\frac{H_T}{w}$ is almost linear with respect to $\frac{H_A}{w}$. In Figure 3, a straight line e_1e_2 is marked across the numerical data and this straight line is given by

$$\begin{cases} \frac{H_T}{H_A} = -1.0314\frac{g}{H_A} + 0.7227, R^2 = 0.9994 \\ \frac{H_T}{w} = -0.3087\frac{g}{w} + 0.3054, R^2 = 0.9985 \\ \frac{H_T}{w} = -0.3087\frac{H_A}{w} + 0.4359, R^2 = 0.9985 \end{cases}$$

where R^2 stands for the linear correlation coefficient.

The Mach contours for $M_0 = 4$, $\theta_w = 25°$ and $\frac{g}{H_A} = 0.425, 0.475, 0.525, 0.575$ are displayed in Figure 4a–d. From the Mach contours, we can see how the Mach stem height decreases with increasing $\frac{g}{H_A}$. It is noted that when $\frac{g}{H_A}$ increases, the triple point moves in the downstream direction and the flow duct below the slipline is narrowed.

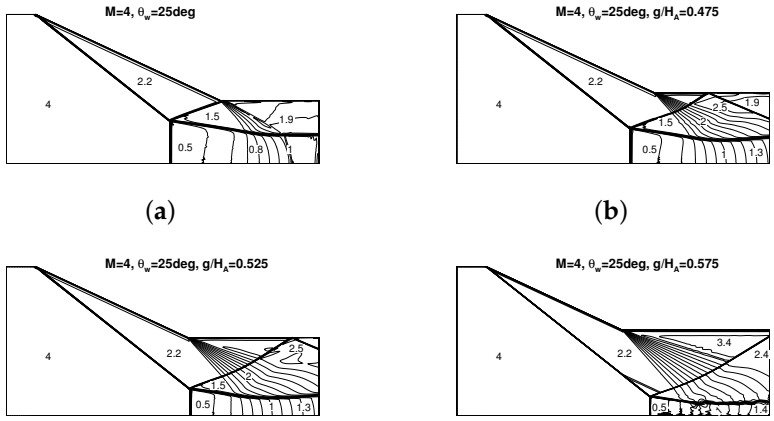

(**a**) (**b**)

(**c**) (**d**)

Figure 4. Numerical results for Mach contours with $M_0 = 4$ and $\theta_w = 25°$: (**a**) $\frac{g}{H_A} = 0.425$; (**b**) $\frac{g}{H_A} = 0.475$; (**c**) $\frac{g}{H_A} = 0.525$; and (**d**) $\frac{g}{H_A} = 0.575$.

The linearity is also observed for another set of M_0 and θ_w. Figure 5a displays the variation of $\frac{H_T}{H_A}$ with respect to $\frac{g}{H_A}$ for $M_0 = 4$, $\theta_w = 30°$ and a set of $\frac{g}{H_A}$ varying from 0.55 to 0.62. Figure 5b displays the variation of $\frac{H_T}{H_A}$ with respect to $\frac{g}{H_A}$ for $M_0 = 3$, $\theta_w = 25°$ and a set of $\frac{g}{H_A}$ varying from 0.57 to 0.70. In Figure 5, a straight line e_1e_2 is marked across the numerical data and this straight line is given by

$$\begin{cases} \frac{H_T}{H_A} = -2.3695\frac{g}{H_A} + 1.6993, R^2 = 0.9996 \\ \frac{H_T}{H_A} = -1.8537\frac{g}{H_A} + 1.4308, R^2 = 0.9990 \end{cases}$$

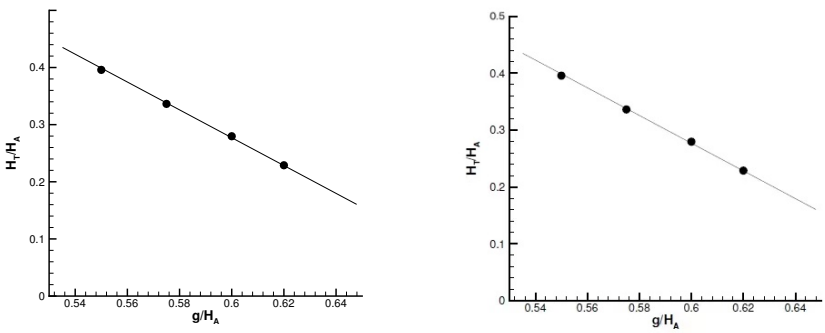

(**a**) (**b**)

Figure 5. Numerical results for normalized Mach stem heights as a function of the normalized wedge trailing edge height: (**a**) $\frac{H_T}{H_A}$ versus $\frac{g}{H_A}$ for $M_0 = 4$ and $\theta_w = 30°$; (**b**) $\frac{H_T}{H_A}$ versus $\frac{g}{H_A}$ for $M_0 = 3$ and $\theta_w = 25°$.

The numerical trend that the normalized Mach stem height decreases with increasing normalized trailing edge height seems to be counter-intuitive (and this trend has been demonstrated by Vuillon, Zeitoun and Ben-Dor [6] for a particular set of conditions), since apparently the Mach stem height should be proportional to the inlet height and one would expect the Mach stem height increase with increasing wedge trailing edge height. However, according to a simplified theoretical analysis given in Section 3, this trend can be justified.

3. A Simplified Analysis Showing Linearity of the Mach Stem Height with Geometry

Analytical models of various degrees of accuracy or complexity have been proposed in the past [16,20–23], none of which have been put into a linear form and have been used to predict the dependence of the Mach stem height on the wedge trailing length. Here,

we derive an expression for the Mach stem height, which can be indeed put into a linear form. This expression is obtained by relating the sonic throat point c to the trailing edge R and to the triple point T, as done in previous works [16,20–23]. This analysis requires the slopes of the shock waves and of the slipline in the vicinity of the triple point as shown in Figure 6, as well as the slopes of the characteristic line Rfc as marked in Figure 1. The method to estimate these slopes is given in Appendix A.

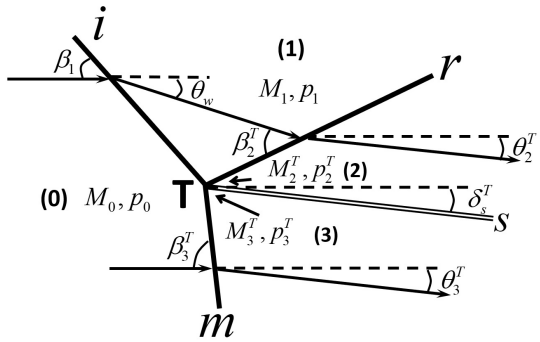

Figure 6. Triple point solution.

3.1. Preliminary Geometric Relations

Here, we establish geometric relations that relate the sonic throat position c to the trailing edge R through the characteristic line Rfc (called the critical characteristic line) and to the triple point T through the slipline Tbc. Notations can be seen in Figure 1. The critical characteristic line brings the required pressure to the sonic throat c on the slipline to balance the critical pressure p^* in the quasi-one-dimensional flow duct below the slipline.

The critical characteristic line Rfc intersects with the reflected shock wave at point f and is composed of two segments Rf and fc, both of which are assumed to be straight as by Bai and Wu [23]. Point f lies on the reflecting shock wave, which is generally curved according to Li and Ben-Dor [16]. Bai and Wu [23] gave a differential relation for the curved shape of this reflected shock. Here, for the purpose of evaluating the position of f within the present context of a simplified analysis, we omit the curvature of the shock segment Tf and relate the position of f to the triple point as

$$y_f - y_T = (x_f - x_T)\tan(\beta_2^T - \theta_w) \tag{1}$$

where β_2^T is the shock angle of the reflected shock wave as shown in Figure 6.

The position of point c at the sonic throat is related to the positions of the intersection point f and the trailing edge R by

$$\begin{cases} y_f - y_R = -(x_f - x_R)S_{Rf} \\ y_c - y_f = -(x_c - x_f)S_{fc} \end{cases} \tag{2}$$

where S_{Rf} is the slope of the critical characteristic line Rf upstream of the reflected shock wave and is determined by

$$S_{Rf} = \tan(\theta_f^* + \mu_f^*) \tag{3}$$

and S_{fc} is the slope of the transmitted critical characteristic line fc which is given by

$$S_{fc} = \tan(\theta_r^* + \mu_r^*). \tag{4}$$

The parameters θ_f^* and μ_f^* are the flow deflection angle and Mach angle along the critical characteristic line Rf. The parameters θ_r^* and μ_r^* are the flow deflection angle and Mach angle along the critical characteristic line fc. The method to evaluate these parameters is given in Appendix A.

Solving (1) and (2) gives the following geometric relation that relates the sonic throat point c to the trailing edge R via the critical characteristic line Rfc :

$$L_1 y_c + L_2 x_c = O_1 y_R + O_2 x_R + N_1 y_T + N_2 x_T, \tag{5}$$

Here:

$$\begin{cases} L_1 = 1 + \frac{S_{fc}}{\Psi} + \frac{\tan(\beta_2^T - \theta_w)}{\Psi} \\ L_2 = S_{fc} + \frac{S_{fc}^2}{\Psi} + \frac{S_{fc}\tan(\beta_2^T - \theta_w)}{\Psi} \\ O_1 = \frac{S_{fc}}{\Psi} + \frac{\tan(\beta_2^T - \theta_w)}{\Psi} \\ O_2 = \frac{S_{Rf} S_{fc}}{\Psi} + \frac{S_{Rf}\tan(\beta_2^T - \theta_w)}{\Psi} \\ N_1 = 1 \\ N_2 = -\tan(\beta_2^T - \theta_w) \end{cases} \tag{6}$$

and:

$$\Psi = \tan(\mu_f^* + \theta_f^*) - \tan(\mu_r^* + \theta_r^*) \tag{7}$$

Now, we establish a geometric relation that relates the sonic throat c to the triple point T through the slipline. This slipline is assumed to be composed of two segments Tb and bc, where b is the intersection of the slipline and the leading characteristics Rab.

Since the intersection point b also lies on the leading characteristics Rab, we have the following geometric relations for point b:

$$\begin{cases} y_a - y_T = (x_a - x_T)\tan(\beta_2^T - \theta_w) \\ y_b - y_a = -(x_b - x_a)\tan(\mu_2^T + \theta_2^T) \\ y_a - y_R = -(x_a - x_R)\tan(\mu_1 + \theta_w) \end{cases} \tag{8}$$

where $\mu_1 = \arcsin\frac{1}{M_1}$ and $\mu_2^T = \arcsin\frac{1}{M_2^T}$ are the Mach angles. Solving (8) yields:

$$l_1 y_b + l_2 x_b = m_1 y_R + m_2 x_R + n_1 y_T + n_2 x_T \tag{9}$$

where:

$$\begin{cases} l_1 = \frac{1}{\Phi_2 \tan(\mu_2^T + \theta_2^T)} + \frac{\tan(\beta_2^T - \theta_w)}{\Phi_1} \\ l_2 = \frac{1}{\Phi_2} + \frac{\tan(\beta_2^T - \theta_w)\tan(\mu_2^T + \theta_2^T)}{\Phi_1} \\ m_1 = \frac{1}{\Phi_2 \tan(\mu_1 + \theta_w)} + \frac{\tan(\beta_2^T - \theta_w)}{\Phi_1} \\ m_2 = \frac{1}{\Phi_2} + \frac{\tan(\mu_1 + \theta_w)\tan(\beta_2^T - \theta_w)}{\Phi_1} \\ n_1 = -1 \\ n_2 = \tan(\beta_2^T - \theta_w) \end{cases} \tag{10}$$

with:

$$\begin{cases} \Phi_1 = \tan(\mu_2^T + \theta_2^T) - \tan(\mu_1 + \theta_w) \\ \Phi_2 = \frac{1}{\tan(\mu_1 + \theta_w)} - \frac{1}{\tan(\mu_2^T + \theta_2^T)} \end{cases} \tag{11}$$

Gao and Wu (2010) found that the segment Tb has some curvature due to secondary expansion waves which serve to balance the pressure change in the quasi-one-dimensional flow duct. Here, we omit this curvature in order to have an explicit relation between c and T. Notations can be seen in Figure 1.

Since b lies on Tb, which is treated to be a straight line, we have:

$$y_T - y_b = (x_b - x_T)\tan\delta_s^T \tag{12}$$

Meanwhile, the slipline bc is a curve that has a vanishing slope at point c (throat). We approximate bc by a second order curve:

$$y - y_b = -(x - x_b)\tan\delta_s^T + \tau(x - x_b)^2 \tag{13}$$

Here, τ is a parameter ensuring that the second order curve has a vanishing slope at point c (throat), i.e., $\left.\frac{dy}{dx}\right|_{x=x_c} = 0$, which, when (13) is used, gives $-\tan\delta_s^T + 2\tau(x_c - x_b) = 0$, or:

$$\tau = \frac{\tan\delta_s^T}{2(x_c - x_b)}$$

Using this value of τ, (13) takes the following simple form:

$$y_c - y_b = -\frac{1}{2}(x_c - x_b)\tan\delta_s^T \tag{14}$$

Solving (12) and (14) gives:

$$\begin{cases} x_b = (y_T - y_c)\frac{2}{\tan\delta_s^T} + 2x_T - x_c \\ y_b = 2y_c - y_T - x_T\tan\delta_s^T + x_c\tan\delta_s^T \end{cases} \tag{15}$$

Now, putting (15) into (9) gives the geometric relation that relates the sonic throat to the triple point via the slipline:

$$X_1 y_c + X_2 x_c = Y_1 y_R + Y_2 x_R + Z_1 y_T + Z_2 x_T \tag{16}$$

where:

$$\begin{cases} X_1 = 2l_1 - \frac{2l_2}{\tan\delta_s^T} \\ X_2 = l_1\tan\delta_s^T - l_2 \\ Y_1 = m_1 \\ Y_2 = m_2 \\ Z_1 = l_1 - \frac{2l_2}{\tan\delta_s^T} + n_1 \\ Z_2 = l_1\tan\delta_s^T - 2l_2 + n_2 \end{cases} \tag{17}$$

In summary, the geometric relation (5) connects the sonic throat c to the trailing edge R following the critical characteristic line, and the relation (16) connects the sonic throat c to the triple point T following the slipline. They will be used to derive the expression for the Mach stem height below.

3.2. Mach Stem Height Expression Showing Linearity

In the following, we will use:

$$y_T = H_T, y_C = H^* = \frac{H_T}{\psi(M_m)}, y_R = g, x_R - x_A = L = \frac{H_A - g}{\tan\theta_w}, x_A = 0, y_A = H_A \tag{18}$$

Here, H^* is the height of the sonic throat which can be related to the Mach stem height H_T by the quasi-one-dimensional area Mach number relation $\frac{H_T}{H^*} = \psi(M_m)$ where:

$$\psi(M_m) = \frac{1}{M_m}\left(\frac{2}{\gamma+1}\left(1 + \frac{\gamma-1}{2}M_m^2\right)\right)^{\frac{\gamma+1}{2(\gamma-1)}} \tag{19}$$

The triple point is on the incident shock wave, so that $y_A - y_T = (x_T - x_A)\tan\beta_1$, meaning that:

$$x_T = x_A + \frac{y_A - y_T}{\tan\beta_1} \tag{20}$$

For $x_A = 0$, the expression (20) simplifies to:

$$x_T = \frac{H_A - H_T}{\tan\beta_1} \tag{21}$$

Solving (5) and (16) gives:

$$Qy_c = C_1 y_R + C_2 x_R + D_1 y_T + D_2 x_T \tag{22}$$

where:

$$\begin{cases} Q = X_2 \frac{L_1}{L_2} - X_1 \\ C_1 = X_2 \frac{O_1}{L_2} - Y_1 \\ C_2 = X_2 \frac{O_2}{L_2} - Y_2 \\ D_1 = X_2 \frac{N_1}{L_2} - Z_1 \\ D_2 = X_2 \frac{N_2}{L_2} - Z_2 \end{cases} \tag{23}$$

Using (21) to replace x_T in (22), we obtain:

$$Qy_c = C_1 y_R + C_2 x_R + \left(D_1 - \frac{D_2}{\tan \beta_1} \right) y_T + D_2 x_A + \frac{D_2}{\tan \beta_1} y_A \tag{24}$$

Putting (18) into (24) yields:

$$\begin{cases} \frac{H_T}{H_A} = A(M_0, \theta_w) \frac{g}{H_A} + B(M_0, \theta_w) \\ A(M_0, \theta_w) = \frac{C_1 - \frac{C_2}{\tan \theta_w}}{\frac{Q}{\psi(M_m)} - D_1 + \frac{D_2}{\tan \beta_1}} \\ B(M_0, \theta_w) = \frac{\frac{C_2}{\tan \theta_w} + \frac{D_2}{\tan \beta_1}}{\frac{Q}{\psi(M_m)} - D_1 + \frac{D_2}{\tan \beta_1}} \end{cases} \tag{25}$$

The expression (25) indeed shows the linearity of $\frac{H_T}{H_A}$ with respect to $\frac{g}{H_A}$, for fixed M_0, θ_w. This linearity has been observed in numerical simulation, as shown in Figure 3a.

If we introduce the obvious geometric relation $H_A = g + w \sin \theta_w$ into (25), we obtain an equivalent form:

$$\begin{cases} \frac{H_T}{w} = D^{(k)}(M_0, \theta_w) \frac{g}{w} + E^{(k)}(M_0, \theta_w) \\ D^{(k)} = A^{(k)}(M_0, \theta_w) + B^{(k)}(M_0, \theta_w) \\ E^{(k)} = B^{(k)}(M_0, \theta_w) \sin \theta_w \end{cases} \tag{26}$$

which shows the linearity of $\frac{H_T}{w}$ with respect to $\frac{g}{w}$, for fixed M_0, θ_w. This linearity was observed in numerical simulation, as shown in Figure 3b.

If we put $g = H_A - w \sin \theta_w$ into (26), we obtain another equivalent form:

$$\frac{H_T}{w} = D^{(k)}(M_0, \theta_w) \frac{H_A}{w} + E^{(k)}(M_0, \theta_w) \tag{27}$$

where $E^{(k)} = B^{(k)}(M_0, \theta_w) \sin \theta_w$. Thus, if normalized inlet height $\frac{H_A}{w}$ is used as an input parameter representing geometry, $\frac{H_T}{w}$ is still a linear function of $\frac{H_A}{w}$, for fixed M_0 and θ_w. This linearity has been observed in numerical simulation, as shown in Figure 3c. Note that Li and Ben-Dor [16] considered a situation where the wedge length w is fixed and the height g is increased, and showed that the foot of the Mach stem follows a linear trajectory. This observation, which they pointed out needs to be explained, may be associated with the linearity pointed out by the present work.

3.3. Assessment of the Accuracy of the Mach Stem Height Expression

The Mach stem height expressions (25)–(27) were obtained under some simplifications as stated in Appendix A. It is thus interesting to see whether these are also accurate enough for quantitative prediction. Here, we will assess their accuracy by comparing them with previous results and the present CFD data.

The experimental data of Hornung and Robinson [18] are usually used for comparison. Here, we consider their case with $M_0 = 3.98$ and $g/w = 0.4$, with the varying incident shock angle (β_1). Figure 7 displays the comparison of the Mach stem height expression (25)

with some various previous works. In Figure 7, the experimental data of Hornung and Robinson [18] and Mouton and Hornung [27], and the CFD data of Mouton and Hornung [21], and Vuillon et al.[6] are displayed. It can be seen that the expression (25) provides a curve lying between the curves of Bai and Wu [23] and Gao and Wu [22].

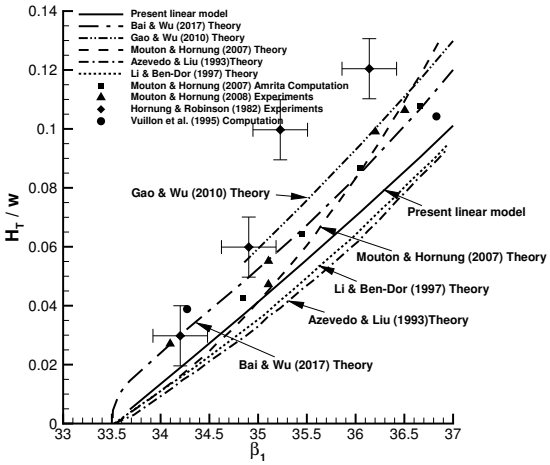

Figure 7. Comparison of the linear model (25) against previous authors for $M_0 = 3.98$ and $g/w = 0.4$.

The comparison of linear expression (25) with the present numerical solutions (already shown in Figure 3a–c and Figure 5a,b of Section 2) is given in Figure 8a–e. It is seen that, though the expression (25) displays linearity as CFD simulation, the slopes of the linear curves signficantly differ from the CFD results.

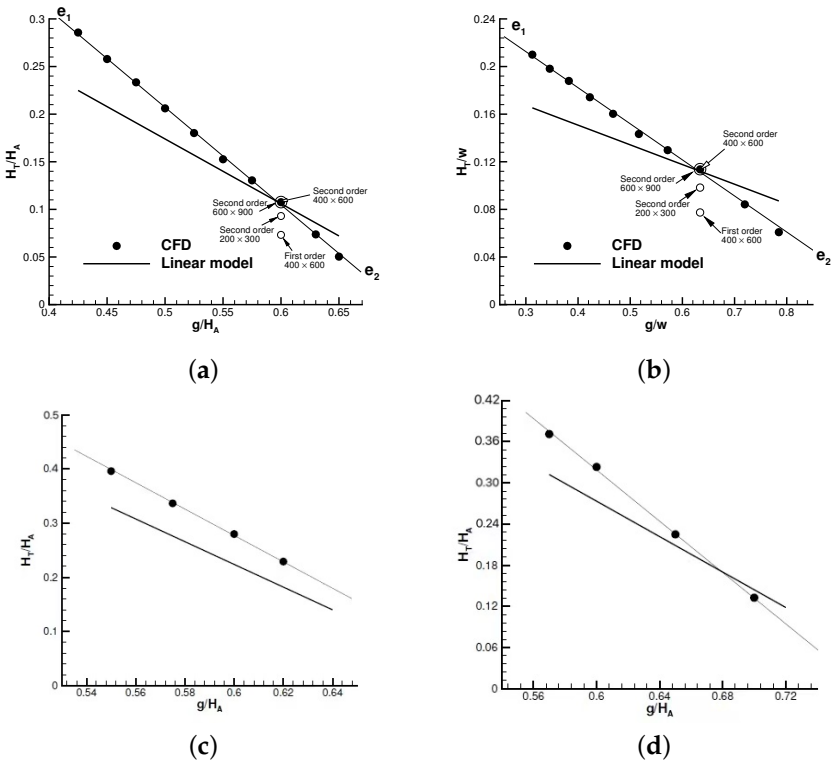

Figure 8. *Cont.*

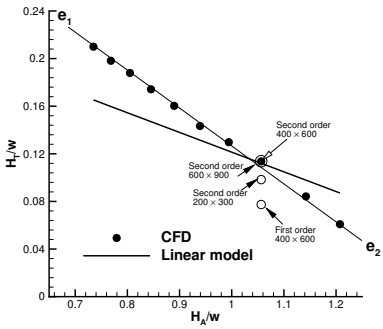

(**e**)

Figure 8. Comparison between the linear model (25) and CFD data: (**a**) $\frac{H_T}{H_A}$ versus $\frac{g}{H_A}$ for $M_0 = 4, \theta_w = 25°$; (**b**) $\frac{H_T}{w}$ versus $\frac{g}{w}$ for $M_0 = 4, \theta_w = 25°$; (**c**) $\frac{H_T}{H_A}$ versus $\frac{g}{H_A}$ for $M_0 = 4, \theta_w = 30°$; (**d**) $\frac{H_T}{H_A}$ versus $\frac{g}{H_A}$ for $M_0 = 3, \theta_w = 25°$; and (**e**) $\frac{H_T}{w}$ versus $\frac{H_A}{w}$ for $M_0 = 4, \theta_w = 25°$.

3.4. Summary and Significance of the Linear Analysis

The linearity predicted in the present simplified analysis appears to suggest that the linearity observed in the CFD simulation for a finite number of input parameters has some generality.

A comparison of the linear model (25) obtained from the simplified analysis of CFD data suggests that the slope, say $\frac{A(M_0,\theta_w)}{B(M_0,\theta_w)}$, in the linear curve does not yet have the required accuracy to be comparable with CFD data. The factors A and B in the expression (25) thus need elaboration before the expression (25) can be used for accurate prediction.

Despite the difference between the slope in the model (25) and the slope in CFD results, the agreement of linearity is meaningful in the future study of model elaboration since in the suggested linear model, the influence of wedge height and the influence of the inflow Mach number M_0 and wedge angle θ_w are separate. For model elaboration, one can focus on working out more accurate A and B, which only depend on the inflow Mach number M_0 and wedge angle θ_w. Moreover, even without knowing the exact values of the linear coefficients A and B, the conclusion that the normalized Mach stem height is linear with respect to the normalized wedge height is already useful in specific application to consider the precise influence of geometry, since one can just perform numerical or experimental work for the two sets of wedge height to fit the values of the slope in the linear model and then apply this linear model to predict the Mach stem height for other wedge height. This could greatly reduce the cost.

4. Conclusions

In this paper, we considered the dependence of the Mach stem height on the geometry when the geometry parameter (such as the trailing edge height) has a wide range. Such a study complements the past studies since many of the previous studies have focused on a narrow range of geometry.

Numerical simulation showed that the normalized Mach stem height is almost linear with respect to the normalized trailing edge height, independently of how they are normalized. When the trailing edge height is increased, keeping the inflow Mach number and the wedge angle fixed, the triple point moves in the downstream direction and the flow region between the slipline and the reflected surface is narrowed.

A simplified analysis showed that the linearity observed in CFD could be explained. This analysis leads to an expression of the normalized Mach stem height with respect to the normalized trailing edge height, which has the linear form $\frac{H_T}{H_A} = A\frac{g}{H_A} + B$ or $\frac{H_T}{w} = A\frac{g}{w} + B$. The coefficients A and B only depend on the inflow Mach number and the wedge angle.

The present work suggested that a Mach stem height model can be expressed as a linear function of the geometry. Further work could be done by working out more accurate coefficients A and B for purpose of quantitative prediction. In a specific application to consider the precise influence of geometry, one can also perform numerical or experimental work for two sets of wedge height to fit the values of the slope in the linear model and then apply this linear model to predict the Mach stem height for other wedge height.

Author Contributions: C.-Y.B. and Z.-N.W. equally contributed to the development of the present paper, including the conceptualization, methodology, data acquisition and analysis, interpretation of the results, and manuscript preparation. All authors have read and agreed to the published version of the manuscript.

Funding: The authors are thankful to the editors and referees who provided valuable comments to improve the manuscript. This work was partly supported by the National Key Project (Grant No. GJXM92579), by the National Science and Technology Major Project 2017-II-003-0015, and by the National Natural Science Foundation of China (Grants No. 11721202).

Institutional Review Board Statement: Not applicable.

Informed Consent Statement: Not applicable.

Data Availability Statement: Not applicable.

Conflicts of Interest: The authors declare no conflict of interest.

Appendix A. Method to Evaluate the Slopes of Shock Waves and Critical Characteristic Line

In this Appendix A, we provide the estimation of the slopes of various waves required in the Mach stem height model presented in Section 3.

Appendix A.1. Slopes of Waves in the Vicinity of Triple Point

The triple point theory, due to von Neumann[28], provides solutions in the vicinity of the triple point (T) as shown in Figure 6. The solutions in regions (1), (2) and (3), in the vicinity of the triple point, follow from the oblique shock wave relations for shock i, r and m:

$$\begin{cases} \tan\theta_w = f_\theta(M_0,\beta_1), M_1^2 = f_M(M_0,\beta_1), p_1 = f_p(M_0,\beta_1)\ (i) \\ \tan(\theta_w - \theta_2^T) = f_\theta(M_1,\beta_2^T), \left(M_2^T\right)^2 = f_M(M_1,\beta_2^T), p_2^T = f_p(M_1,\beta_2^T)\ (r) \\ \tan\theta_3^T = f_\theta(M_0,\beta_3^T), \left(M_3^T\right)^2 = f_M(M_0,\beta_3^T), p_3^T = f_p(M_0,\beta_3^T)\ (m) \end{cases} \tag{A1}$$

Here, the flow parameters in the vicinity of the triple point are denoted with superscript T, and $f_\theta(M,\beta), f_M(M,\beta), f_p(M,\beta)$ are functions for oblique shock waves defined by

$$\begin{cases} f_\theta(M,\beta) = 2\cot\beta\frac{M^2\sin^2\beta-1}{M^2(\gamma+\cos 2\beta)+2} \\ f_M(M,\beta) = \frac{M^2+\frac{2}{\gamma-1}}{\frac{2\gamma}{\gamma-1}M^2\sin^2\beta-1} + \frac{M^2\cos^2\beta}{\frac{\gamma-1}{2}M^2\sin^2\beta+1} \\ f_p(M,\beta) = \frac{2\gamma}{\gamma+1}M^2\sin^2\beta - \frac{\gamma-1}{\gamma+1} \end{cases} \tag{A2}$$

For shock i and r, the oblique shock wave relations are solved for weak solutions (i.e., for the smaller value of shock angle β). For shock m, the oblique shock wave relations are solved for strong solution (i.e., for the larger value of shock angle β).

Across the slipline, the flow streams are parallel, i.e.,

$$\theta_3^T = \theta_2^T = \delta_s^T \tag{A3}$$

and the pressures are balanced, meaning that:

$$p_2^T = p_3^T \tag{A4}$$

Giving M_0 and θ_w, Equations (A1)–(A4) form a closed set to determine the flow parameters near the triple point, i.e., the Mach numbers M_2^T, M_3^T, the pressures $p_2^T = p_3^T$, the initial shock angle β_2^T of the reflected shock wave and the initial angle of the slipline δ_s^T. The shock angle β_2^T and the slipline angle δ_s^T were used in Equations (6) and (17) to establish the required geometrical relations for the Mach stem height model.

Appendix A.2. Slopes of the Critical Characteristic Line

In order to compute the slopes S_{Rf} and S_{fc} of the critical characteristic line Rfc by Equations (3) and (4), we need to evaluate θ_f^*, μ_f^*, θ_r^* and μ_r^*. Here, θ_f^* is the local flow deflection angle inside the trailing edge expansion fan, at which the pressure p_f^*, when amplified through the reflected shock wave to become p_r^*, will be carried out through the critical characteristic line fc to the sonic throat to balance the critical pressure p_s^* (pressure at the sonic throat in the quasi-one-dimensional flow duct), meaning that:

$$p_r^* = p_s^* \tag{A5}$$

The critical pressure p_s^* can be determined by using an isentropic flow assumption for pressure. This gives a relation between the pressure p_s^* at the sonic point ($M_s^* = 1$) and the pressure p_m behind the Mach stem:

$$\frac{p_s^*}{p_m} = \left(\frac{1 + \frac{\gamma-1}{2} M_m^2}{1 + \frac{\gamma-1}{2}} \right)^{\frac{\gamma}{\gamma-1}}. \tag{A6}$$

where M_m is the Mach number behind the Mach stem. The parameters p_m and M_m can be computed as $p_m = \frac{1}{2}(p_3^T + p_n)$, $M_m = \frac{1}{2}(M_3^T + M_n)$, where p_n and M_n are normal shock solutions computed as $p_n = f_p(M_0, \frac{\pi}{2})$, $M_n^2 = f_M(M_0, \frac{\pi}{2})$.

The amplified pressure p_r^*, the pressure along the critical characteristic line fc, depends on the interaction between the expansion fan and the reflected shock wave. Bai and Wu [23] gave a differential form to predict this. Here, within the present context of simplicity, we assume that $p_r^* = \frac{p_2^T}{p_1} p_f^*$, i.e., the pressure at point f, is amplified by the reflected shock wave by the same factor as through the initial segment Ta of the reflected shock wave.

Using (A5), $p_r^* = \frac{p_2^T}{p_1} p_f^*$, and (A6), we obtain:

$$p_f^* = \left(\frac{1 + \frac{\gamma-1}{2} M_m^2}{1 + \frac{\gamma-1}{2}} \right)^{\frac{\gamma}{\gamma-1}} \frac{p_1 p_m}{p_2^T} \tag{A7}$$

which is the pressure at $\theta = \theta_f^*$. This pressure is further related to the pressure p_1 in region (1) by the Prandtl–Meyer relation:

$$\begin{cases} p_f^* = \left(\frac{1 + \frac{\gamma-1}{2} M_1^2}{1 + \frac{\gamma-1}{2} M_f^{*2}} \right)^{\frac{\gamma}{\gamma-1}} p_1 \\ \nu(M_f^*) - \nu(M_1) = \theta_w - \theta_f^* \end{cases}. \tag{A8}$$

where $\nu(M) = \sqrt{\frac{\gamma+1}{\gamma-1}} \arctan \sqrt{\frac{\gamma-1}{\gamma+1}(M^2 - 1)} - \arctan \sqrt{M^2 - 1}$ is the Prandtl–Meyer function. Once (A7) is used to obtain p_f^*, the first expression in (A8) is used to obtain the Mach number M_f^* and the last expression in (A8) is used to obtain θ_f^*. The Mach angle μ_f^* can then by computed through $\sin \mu_f^* = 1/M_f^*$. These provide values of θ_f^* and μ_f^*, needed in (3), to compute the slope of the segment Rf of the critical characteristic line.

By (A5) and by (A6), we obtain:

$$p_r^* = \left(\frac{1 + \frac{\gamma-1}{2} M_m^2}{1 + \frac{\gamma-1}{2}} \right)^{\frac{\gamma}{\gamma-1}} p_m$$

We then consider the oblique shock wave relation across the reflected shock wave at point f. After solving the pressure relation $p_r^* = f_p\left(M_f^*, \beta_r^*\right)$ to obtain the local shock angle β_r^*, we then solve $\tan(\theta_r^* - \theta_f^*) = f_\theta\left(M_f^*, \beta_r^*\right)$ to obtain the local flow deflection angle θ_r^*, and then solve $M_r^{*2} = f_M\left(M_f^*, \beta_r^*\right)$ to obtain the Mach number M_r^*, before finally using $\sin \mu_r^* = 1/M_r^*$ for the Mach angle. These provide values of θ_r^* and μ_r^*, needed in (4), to compute the slope of the segment fc of the critical characteristic line.

References

1. Ben-Dor, G. *Shock Wave Reflection Phenomena*; Springer: Berlin/Heidelberg, Germany, 2007.
2. Henderson, L.F.; Lozzi, A. Experiments on transition of Mach reflection. *J. Fluid Mech.* **1975**, *68*, 139–155. [CrossRef]
3. Bazhenova, T.V.; Fokeev, V.P.; Gvozdeva, L.G. Regions of various forms of Mach reflection and its transition to regular reflection. *Acta Astronaut.* **1976**, *3*, 131–140. [CrossRef]
4. Hornung, H.G.; Oertel, H.; Sandeman, R.J. Transition to Mach reflection of shock waves in steady and pseudo-steady flows with and without relaxation. *J. Fluid Mech.* **1979**, *90*, 541–560. [CrossRef]
5. Teshukov, V.M. On stability of RR of shock waves. *Prikl. Mekh. Technol. Fiz* **1989**, *2*, 26–33.
6. Vuillon, J.; Zeitoun, D.; Ben-Dor, G. Reconstruction of oblique shock wave reflection in steady flows. Part 2. Numerical investigation. *J. Fluid Mech.* **1995**, *301*, 37–50 . [CrossRef]
7. Chpoun, A.; Passerel, D.; Li, H.; Ben-Dor, G. Reconsideration of the oblique shock wave reflection in steady flows. Part 1. Experimental investigation. *J. Fluid Mech.* **1995**, *301*, 19–35. [CrossRef]
8. Li, H.; Ben-Dor, G. Application of the principle of minimum entropy production to shock wave reflections. I. Steady flows. *J. Appl. Phys.* **1996**, *80*, 2027–2037. [CrossRef]
9. Ivanov, M.S.; Ben-Dor, G.; Elperin, T.; Kudryavtsev, A.N.; Khotyanovsky, D.V. Flow–Mach-number-variation-induced hysteresis in steady flow shock wave reflections. *AIAA J.* **2001**, *39*, 972–974. [CrossRef]
10. Ben-Dor, G.; Ivanov, M.; Vasilev, E.I.; Elperin, T. Hysteresis processes in the regular reflection to Mach reflection transition in steady flows. *Prog. Aerosp. Sci.* **2002**, *38*, 347–387. [CrossRef]
11. Hornung, H. Mach reflection in steady flow. I. Mikhail Ivanovs contributions, II. Caltech stability experiments. *AIP Conf. Proc. AIP Publ.* **2014**, *1628*, 1384–1393.
12. Courant, R.; Friedrichs, K.O. *Supersonic Flow and Shock Waves*; Wiley-Interscience: Hoboken, NJ, USA, 1948.
13. Liepmann, H.; Roshko, A. *Elements of Gasdynamics*; John Wiley and Sons: Hoboken, NJ, USA, 1957.
14. Emanuel, G. *Gasdynamics: Theory and Applications*; American Institute of Aeronautics and Astronautics: New York, NY, USA, 1986.
15. Ben-Dor, G.; Takayama, K. The phenomena of shock wave reflection-a review of unsolved problems and future research needs. *Shock Waves* **1992**, *2*, 211–223. [CrossRef]
16. Li, H.; Ben-Dor, G. A parametric study of Mach reflection in steady flows. *J. Fluid Mech.* **1997**, *341*, 101–125. [CrossRef]
17. Chow, W.L.; Chang, I.S. Mach reflection associated with over-expanded nozzle free jet flows. *AIAA J.* **1975**, *13*, 762–766. [CrossRef]
18. Hornung, H.G.; Robinson, M. Transition from regular to Mach reflection of shock waves Part 2. The steady-flow criterion. *J. Fluid Mech.* **1982**, *123*, 155–164. [CrossRef]
19. Schmisseur, J.; Gaitonde, D. Numerical simulation of Mach reflection in steady flows. *Shock Waves* **2011**, *21*, 499–509. [CrossRef]
20. Azevedo, D.J.; Liu, C.S. Engineering approach to the prediction of shock patterns in bounded high-speed flows. *AIAA J.* **1993**, *31*, 83–90. [CrossRef]
21. Mouton, C.A.; Hornung, H. Mach stem height and growth rate predictions. *AIAA J.* **2007**, *45*, 1977–1987. [CrossRef]
22. Gao, B.; Wu, Z.N. A study of the flow structure for Mach reflection in steady supersonic flow. *J. Fluid Mech.* **2010**, *656*, 29–50. [CrossRef]
23. Bai, C.Y.; Wu, Z.N. Size and shape of shock waves and slipline for Mach reflection in steady flow. *J. Fluid Mech.* **2017**, *818*, 116–140. [CrossRef]
24. Roy, S.; Gopalapillai, R. An analytical model for asymmetric Mach reflection configuration in steady flows. *J. Fluid Mech.* **2019**, *863*, 242–268. [CrossRef]
25. Lin, J.; Bai, C.Y.; Wu, Z.N. Study of asymmetrical whock wave reflection in steady supersonic flow. *J. Fluid Mech.* **2019**, *864*, 848–875. [CrossRef]
26. Roe, P. Characteristic based schemes for the Euler equations. *Annu. Rev. Fluid Mech.* **1986**, *18*, 337–365. [CrossRef]
27. Mouton, C.A.; Hornung, H. Experiments on the mechanism of inducing transition between regular and Mach reflection Mach stem height and growth rate predictions. *Phys. Fluids* **2008**, *20*, D541–D572. [CrossRef]
28. Von Neumann, J. *Oblique Reflection of Shock*; Explos. Res. Rep. 12 Navy Dept.; Bureau of Ordinance: Washington, DC, USA, 1943.